Al-Rafidain Journal of Engineering Sciences

Journal homepage https://rjes.iq/index.php/rjes

ISSN 3005-3153 (Online)

Numerical Study on the Shear Capacity-Curvature Ductility Relationship of High Strength Reinforced Concrete Beams under Different Failure Modes Using ABAQUS

Hussein A. Merie[1]*, Mazin B. Abdulrahman[2]

[1,2]Civil Department, Engineering College, Tikrit University، Tikrit, Iraq

ARTICLE INFO

Article history:
Received 26 September 2024
Revised 27 September 2024,
Accepted 10 October 2024,
Available online 12 October 2024

Keywords:
Cantilever beam,
Curvature ductility,
High-strength concrete,
Shear capacity,
Mode of failure,
ABAQUS.

ABSTRACT

Studying shear capacity in reinforced concrete beams is vital for structural safety and integrity. Preventing sudden shear failure is essential to avoid catastrophic collapses and ensure reliable construction performance. ABAQUS is vital for the thorough analysis of concrete specimens, offering deeper insights into their behavior under different experimental conditions. This paper explored the correlation between shear capacity and curvature ductility in high-strength reinforced concrete cantilever beams subjected to monotonic loading, involving tests on six cantilever beams with cross sections measuring 200 mm by 300 mm. The study examined how span-to-effective depth ratios ("a/d") and stirrup spacing influence beam behavior at the plastic hinge under various failure modes: flexural, shear, and combined. The specimens were categorized into two groups, with each group comprising 3 beams and 3 values for each variable. In the first test group, as the a/d ratio increased from 750 to 850 and then to 1150 mm, shear capacity increased by 99.3% and 16.3%, while curvature ductility improved by 45.5% and 29.7%. The failure modes included shear, combined, and flexural, indicating a direct yet non-linear relationship between curvature ductility and shear capacity. Increasing stirrup spacing from 100 to 150 and then to 300 resulted in a 37.3% and 59.2% decrease in shear capacity and an 18% and 58.8% reduction in curvature ductility. This demonstrates an inverse non-linear relationship and a shift in failure mode from flexural to combined and then to shear.

1. Introduction

Shear capacity in reinforced concrete (RC) beams refers to their ability to resist shear forces, preventing sliding failure. This capacity is affected by concrete strength, cross-sectional shape, and reinforcement type. Common failure modes include diagonal tension failure, characterized by angled cracks, and shear-compression failure, where concrete in the compression zone fails under high shear. Adding stirrups is vital for enhancing shear capacity, as they control crack spread and increase strength. Exceeding this capacity can cause sudden, brittle failures, making understanding shear behavior essential in RC design and analysis [1].

Several factors limit the shear capacity of reinforced concrete (RC) beams under repeated loads. Diagonal cracks weaken shear capacity, while compression zone crushing can exacerbate this. Widened cracks reduce aggregate interlock and shear strength. Corrosion of longitudinal bars and stirrups weakens steel, lowering tensile resistance. Fatigue can degrade the concrete-steel bond, causing slippage and further reducing shear resistance. Overall, cyclic loading leads to deterioration in both concrete and reinforcement, resulting in reduced shear capacity [2].

* Corresponding author E-mail address: enghama28@gmail.com
https://doi.org/10.61268/ybj42c79

In continuous and cantilever beams, plastic hinges form in areas where bending stresses are the strongest, usually near supports and where bending moments are highest. When shear stresses occur along with these bending stresses, the area around the plastic hinge experiences greater stress. This can lead to earlier yielding or failure, particularly in regions with high shear [3]. Table 1 presents several empirical models that define the plastic hinge length (Lp). This length indicates the region where uniform plastic curvature is assumed, which helps in evaluating the flexural deflection and plastic rotation of reinforced concrete (RC) elements.

Table 1. Empirical Models for Plastic Hinge Length

References	Plastic hinge length (L_p)
Baker [4]	$c_0(z/d)^{1/4}d$ (for RC beams and columns)
Sawyer [5]	$0.25d + 0.075z$ (for RC beams)
Corley [6]	$0.5d + 0.2\sqrt{d}(z/d)$ (for RC beams)
Mattock [7]	$0.5d + 0.05z$(for RC beams)
Paulay and [8]	$0.08z + 0.022d_b f_y$(for RC beams and columns)
Panagiotakos and Fardis [9]	$0.18z + 0.021d_b f_y$(for RC beams and columns)

The combination of shear and flexural stresses in the plastic hinge region of RC beams creates complex stress conditions, leading to bending deformations and shear cracks. This can diminish ductility and result in premature failure if shear strength is inadequate. Proper detailing of stirrups and longitudinal reinforcement is crucial to preserve beam integrity [10].

Curvature in reinforced concrete beams quantifies the bending of the beam under load and is defined mathematically as the rate of change of its slope [11]. It is commonly measured experimentally by examining deflection and strain distribution along the beam. Strain gauges positioned at various points record deformation, from which curvature can be calculated [12].

ABAQUS, a Finite Element (FE) software, was used to analyze the performance of reinforced concrete (RC) beams under different parameters. It offers a wide range of elements and material properties, allowing for the simulation of various geometries and both linear and nonlinear behaviors typical of engineering materials [13].

Concrete is a composite material extensively utilized in engineering constructions. Laboratory research indicates that concrete exhibits a pronounced nonlinear response when subjected to uniaxial compression. Consequently, accurate modeling of reinforced concrete (RC) necessitates consideration of this nonlinear behavior [14].

2. Experimental work

This study comprises two main components: a practical investigation and an analytical study using the ABAQUS program. The practical aspect involved examining six samples divided into two groups, each assessing the effect of a different variable. The first group analyzed how varying the shear span to effective depth ratio (2.82, 3.19, and 4.32) influenced the results, while the second group evaluated the impact of stirrups spacing for shear reinforcement at three distances (100, 150, and 300 mm). The focus was on the shear capacity within a defined plastic joint region,

specifically a 300 mm patch from the joint towards the load application point. Each sample underwent monotonic loading, and deflection measurements were taken at the cantilever tip. Subsequently, these samples were simulated in ABAQUS based on their practical test results and failure patterns to explore the theoretical aspect of shear capacity, its relationship with the studied variables, curvature measurements in the targeted area, and the correlation between shear capacity and curvature. Figure 1 displays a sample under examination.

Figure 1. Sample under testing.

3. Input Data

The Concrete Smeared Cracking (CSC) and Concrete Damaged Plasticity (CDP) constitutive models are both available in ABAQUS. The CDP model is preferred over the CSC model due to its superior stability. Widely utilized in various loading conditions, the CDP model effectively characterizes the mechanical behavior of reinforced concrete (RC) and is implemented in the present study.

Table 2 lists the material characteristics of the examined specimens, including concrete and steel reinforcement ratios. This study utilizes six reinforced concrete cantilever beams divided into two groups of three. The first group examines the impact of varying the shear span to effective depth ratio (a/d), while the second group focuses on altering stirrup spacing. Figure. 2 and 3 illustrate the details and geometry of the samples.

Table 2. Specimen details and material properties.

Group No.	Specimens	Shear Span a (mm)	Comp. Strength $f'c$ (MPa)	Longitudinal Tensile R. (#bar)	Transverse R. (Stirrups spacing) (mm)	Target Failure Mode
A	Aa115	1150	65	3Ø16	300	Flexural
	Aa85	850	65	3Ø16	300	combined
	Aa75	750	65	3Ø16	300	Shear
B	Bs30	750	65	3Ø16	300	Shear
	Bs15	750	65	3Ø16	150	combined
	Bs10	750	65	3Ø16	100	Flexural

Note: that for all specimens, height (h) is 266 mm, b is 200 mm, and d is 266 mm, for longitudinal steel f_y is 600 MPa, and for stirrups steel is 550 MPa.

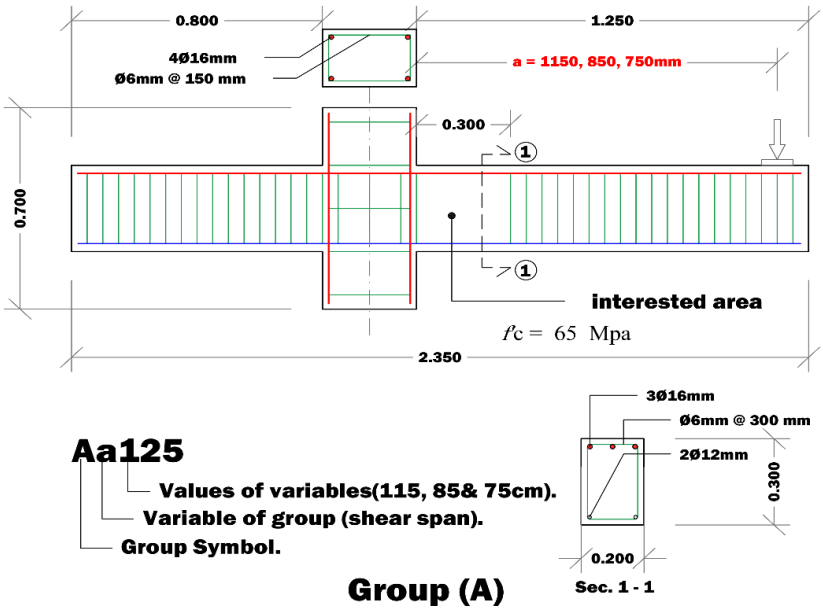

Figure 2. Details and geometry of group (A) samples.

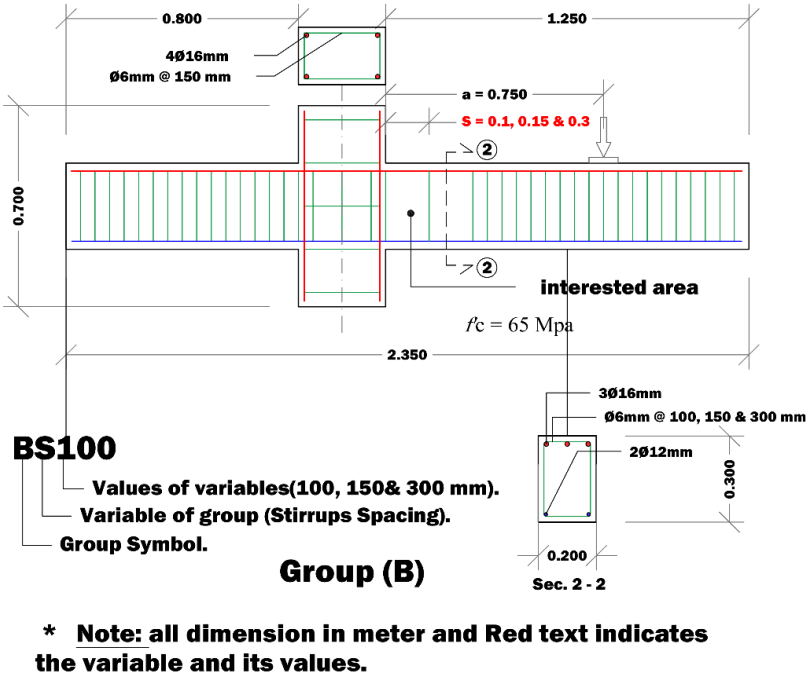

Figure 3. Details and geometry of group (B) samples.

The CDP model requires defining five parameters including:

1. The eccentricity of the hyperbolic flow potential (ε) indicates the point at which the hyperbolic flow potential approaches its asymptote. In ABAQUS, the default value is set to 0.1[15].
2. The viscosity parameter, specifically the relaxation time of the viscous system, is set to a default value of zero in ABAQUS. However, to enhance convergence in certain problems, it may be beneficial to assign a small positive value [16].

3. The ratio of the second stress invariant in the tensile meridian to that in the compressive meridian, with maximal principal stress at (-kc), is a parameter for defining the yield surface of the concrete plasticity model. ABAQUS defaults kc to 0.667 [17], while test results indicate kc ranges from 0.5 to 1.
4. The initial equiaxial compressive yield stress is divided by the initial uniaxial compressive yield stress (fb_o/fc_o), with a default value of 1.16 in ABAQUS [17].
5. The dilation angle (ψ) represents the inclination of plastic potential under confining pressure. In ABAQUS, ψ can range from 0° to 56°. Lower values lead to more brittle concrete behavior. This research selected a dilation angle of 31° [18].

4. Geometric Modelling

All finite element models for this investigation were assembled in four parts.

- The length of the beam and the dimensions of the concrete section.
- Longitudinal steel reinforcement of the beam.
- Stirrups reinforcement of the beam.
- Steel plate for load and support.

The preliminary phase in the fabrication of the components involved creating detailed cross-sectional sketches of each beam. A three-dimensional solid model was utilized to depict the concrete beam, while a three-dimensional wireframe representation was employed to simulate the steel reinforcement.

5. Sample modeling element mesh size.

After the Assembly module, the optimal mesh size for the reinforced concrete beam models was selected for computational efficiency and alignment with experimental results. The concrete element size was set to 30mm cubes, while the mesh size for the main steel bars and stirrups was 25mm.

6. Surface Interactions

Modeling interactions between components is crucial for result accuracy. In this study, steel reinforcement and stirrups were modeled with a perfect bond to surrounding concrete using the "embedded region" option in ABAQUS. The interaction between concrete and loading plates was modeled with a "tie" constraint, while concrete supports used the "Penalty" friction method with a coefficient of 0.74. This ensures full attachment and continuous action during analysis.

7. Load Application and Boundary Conditions

The load was applied to the top surface of the steel loading plates, covering an area of 100 mm by 200 mm, with a vertical downward displacement that matched the displacement recorded from the simulated practical model. The plates' positions were set according to the required shear span for each specimen in the reinforced concrete beam experiment. The sample is supported by a stable chassis on the ground. The first upper support is a 15 mm thick, 200 mm wide, and 900 mm high steel plate shaped like an inverted U, which prevents movement during adjustments. It is securely fastened to the chassis with screws. The second support is similar but shorter, at 700 mm, and secures the end of the continuous beam. All supports are fixed and immovable in the X, Y, or Z directions due to set boundary conditions, illustrated in Figure. 4.

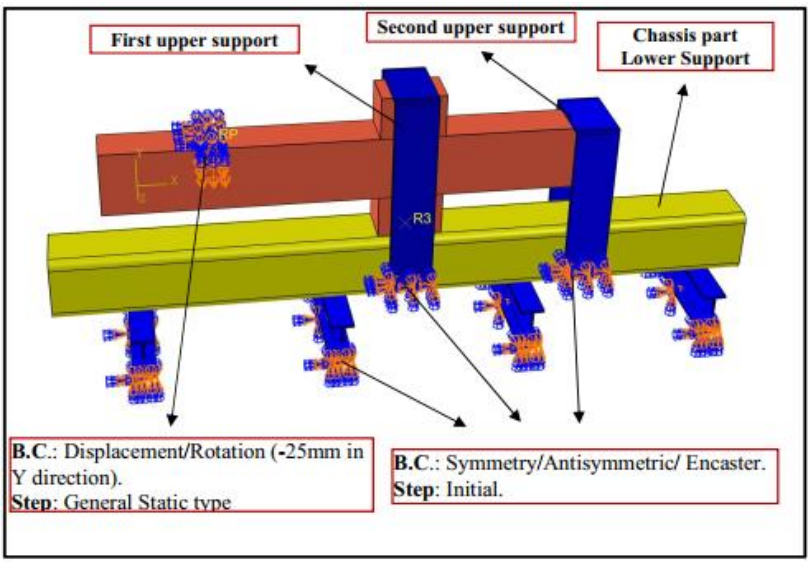

Figure 4. The boundary conditions positions and their types.

8. Finite Element Analysis Results

The results obtained from the finite element analysis of the reinforced concrete beams are summarized in terms of maximum loads and deflections occurring at the point of load application, as detailed in Table 3.

Table 3. Summarizing the finite element results for all tested beams.

Group	Specimen	Ultimate Load (kN)		FE/EXP. Ultimate Load Ratio	Deflection at Tip End (mm)		FE/EXP. Deflection Ratio	Failure Modes
		EXP.	FE		EXP.	FE		
A	Aa75	139.7	125.5	0.90	34	29	0.85	Shear
	Aa85	127.4	121.5	0.95	61	45.5	0.75	Combined
	Aa115	98.6	90.11	0.91	73.22	75.3	1.03	Flexural
B	Bs100	140	126.2	0.90	47.5	45.2	0.95	Flexural
	Bs150	129.2	112.4	0.87	67.8	63.9	0.94	Combined
	Bs300	126.3	122	0.97	37.5	27.7	0.74	Shear

9. Numerical Load-Deflection Response Curves

Experimental test results align closely with the FE analysis in Figures 5 and 6, with the ultimate load capacity 1.2% higher than ABAQUS predictions. There was a 1.3% discrepancy between the experimental and numerical deflection values at ultimate loads, indicating that the constitutive models accurately captured the failure mechanisms of the reinforced concrete beams.

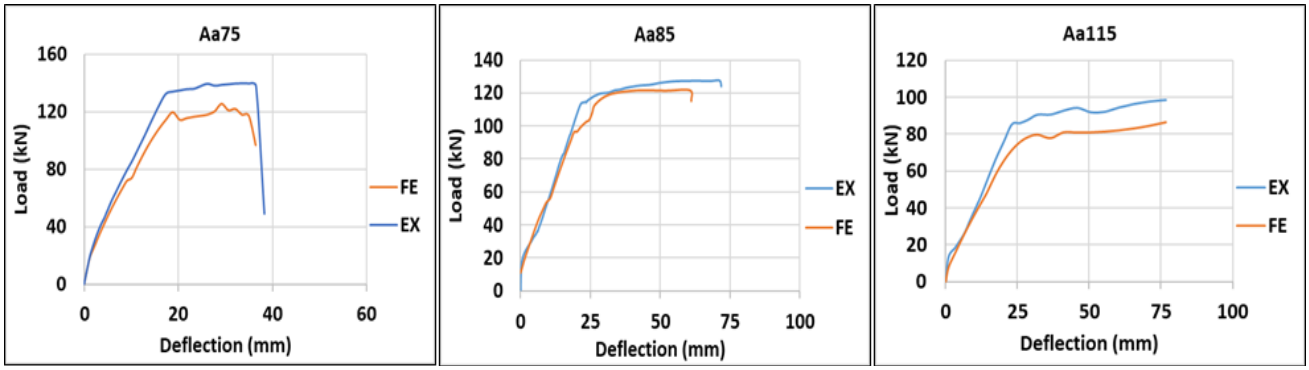

Figure 5. Numerical and experimental load-deflection responses of group (A) samples.

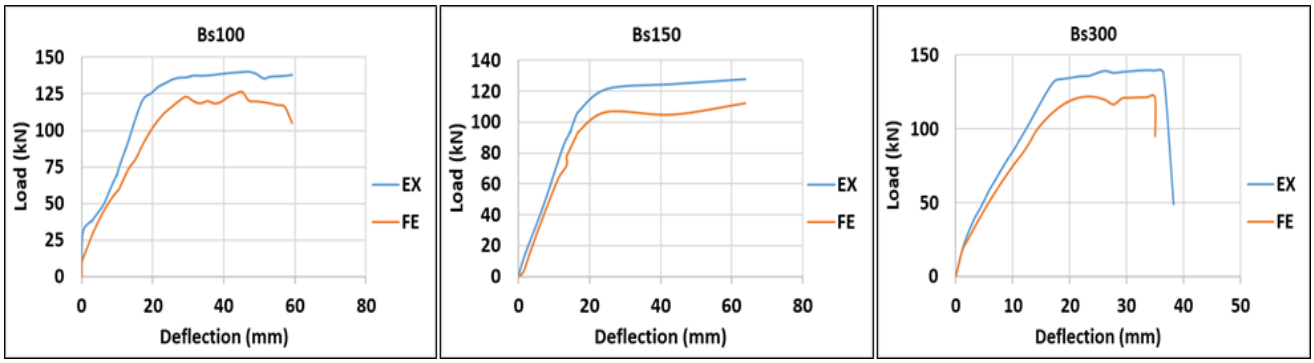

Figure 6. Numerical and experimental load-deflection responses of group (B) samples.

10. Modes of Failure of the Analyzed RC Beams

Figures 7 to 12 illustrate the reinforced concrete beams' failure modes based on experimental results and numerical predictions. The finite element analyses showed that flexural and diagonal cracks occur due to tensile splitting in the struts when they are under load, specifically where the tensile stresses surpass the strength of the concrete. Overall, there is a significant agreement between the numerical predictions and the experimental observations.

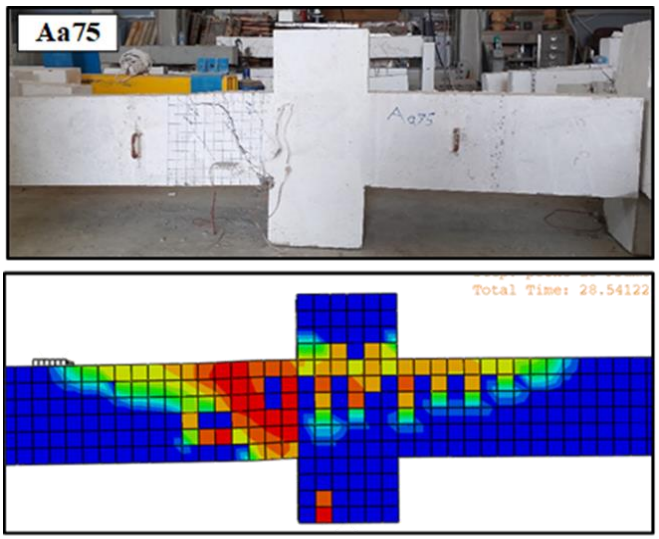

Figure 7. Failure modes of beam Aa75 from tests FE and analysis.

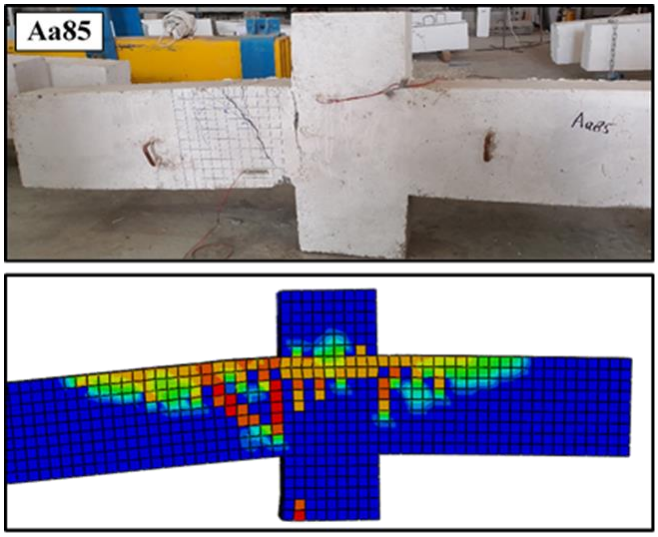

Figure 8. Failure modes of beam Aa85 from tests FE and analysis.

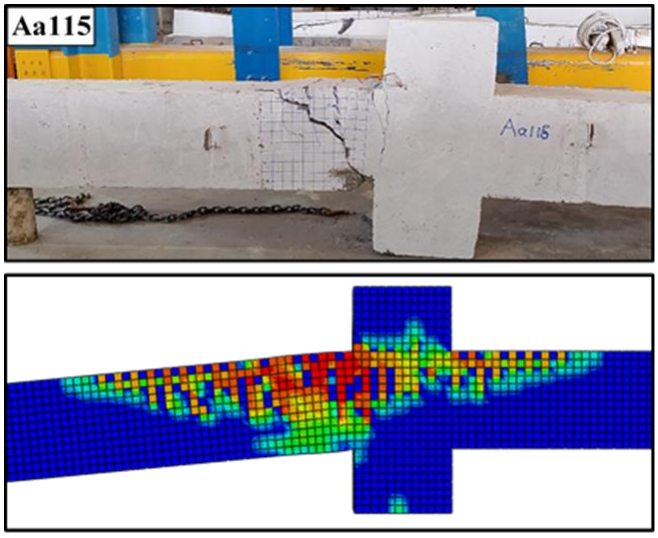

Figure 9. Failure modes of beam Aa115 from tests FE and analysis.

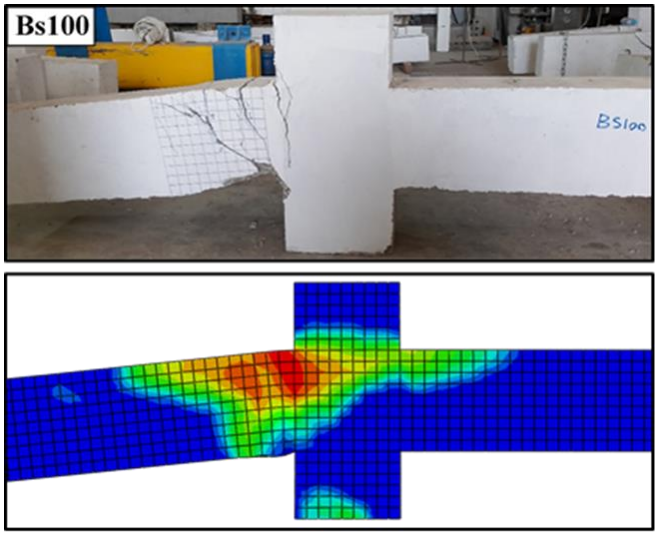

Figure 10. Failure modes of beam Bs100 from tests FE and analysis.

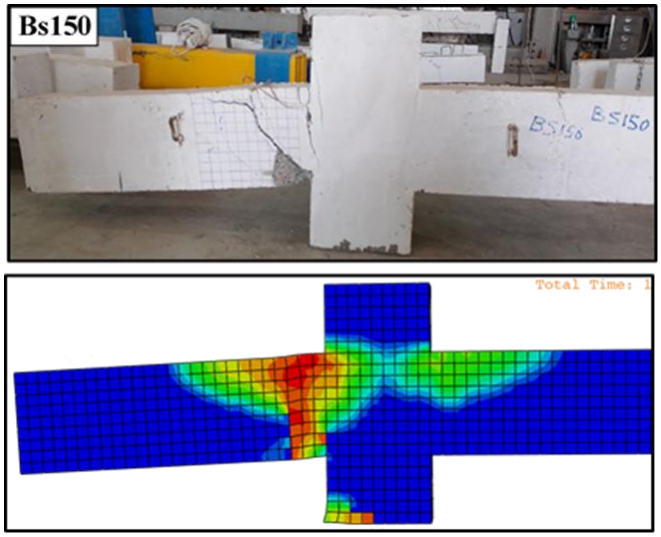

Figure 11. Failure modes of beam Bs150 from tests FE and analysis.

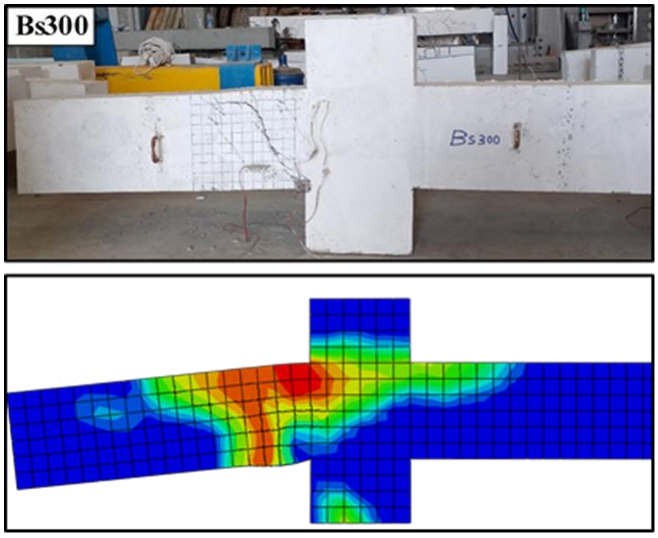

Figure 12. Failure modes of beam Bs300 from tests FE and analysis.

11. Distribution of Reinforcement Stresses

The concrete displayed elastic behavior until reaching full tensile strength, after which it entered a plastic state and began to crack. We analyzed the maximum principal and shear stress distributions in the plastic hinge region of the loading beams. In the ABAQUS program, group (A) beams had shear spans of 750, 850, and 1150 mm, affecting the maximum stresses. In contrast, group (B) beams had stirrup spacing of 100, 150, and 300 mm, which influenced stresses in the reinforced concrete beams, as illustrated in Figures 13 to 18. The Von Mises yield criterion (S, Mises in ABAQUS) effectively determines rebar yield or failure, accurately identifying yield points under multiaxial stress conditions, especially for ductile materials like steel [19].

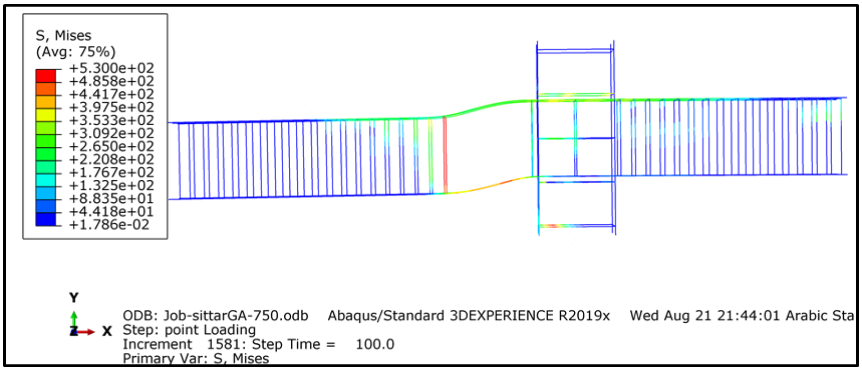

Figure 13. Maximum principal and shear stress of the beam Aa75**.**

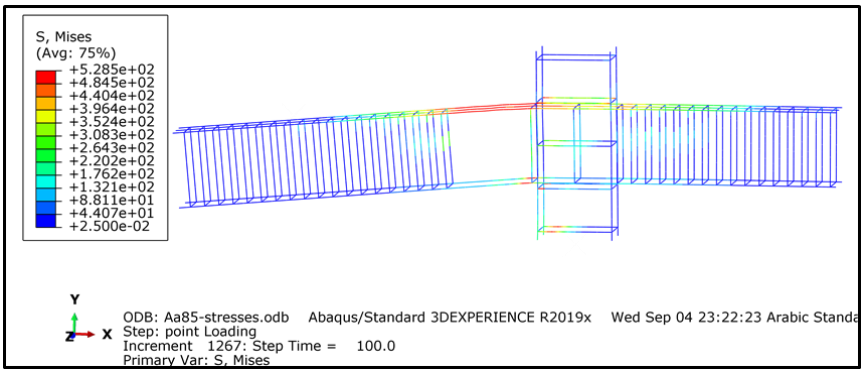

Figure 14. Maximum principal and shear stress of the beam Aa85.

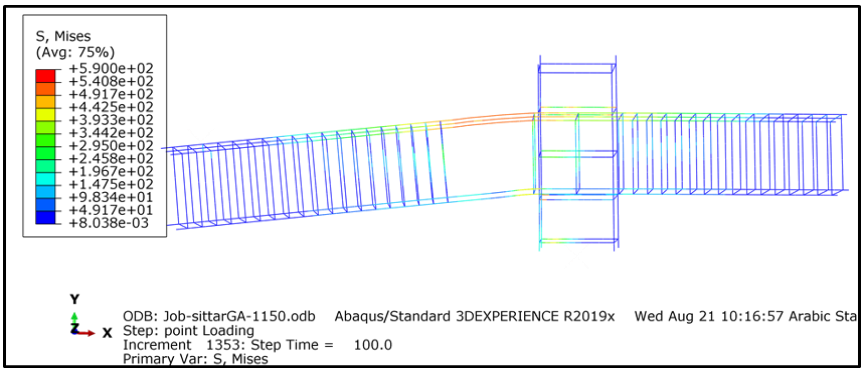

Figure 15. Maximum principal and shear stress of the beam Aa115.

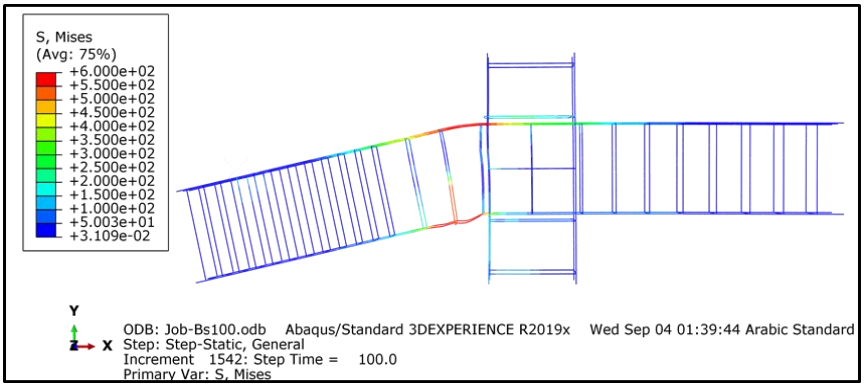

Figure 16. Maximum principal and shear stress of the beam Bs100.

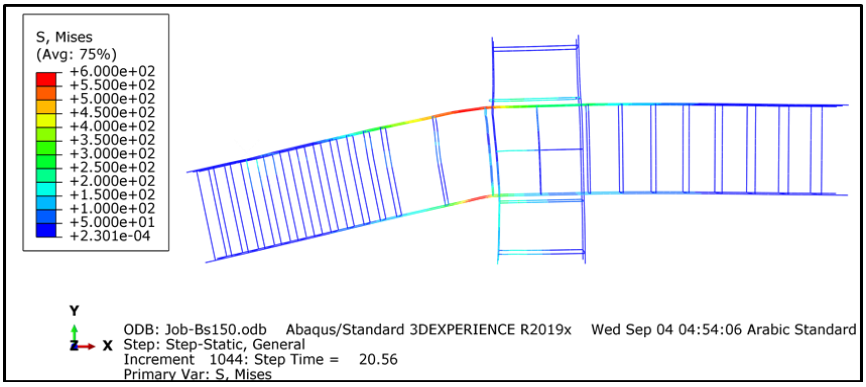

Figure 17. Maximum principal and shear stress of the beam Bs150.

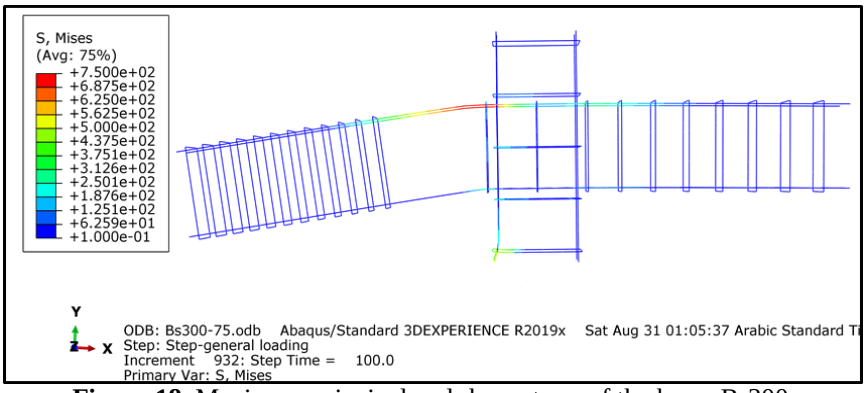

Figure 18. Maximum principal and shear stress of the beam Bs300.

12. Shear Capacity Assessment

Assessing the shear capacity of reinforced concrete beams in ABAQUS is simple, as the software provides essential parameters like stress, strain, and displacement throughout the specimen. The shear capacity is mainly affected by concrete strength and transverse reinforcement (stirrups), which are evaluated separately as detailed below.

12.1 Concrete Shear Strength

Shear stresses are determined from the S12 stress components, reflecting shear effects of applied loads. ABAQUS post-processing tools help visualize shear stress distribution in the beam. Values in the target area are compared to ACI218-19 standards (Equation.1); exceeding them indicates failed concrete resistance. Figure 19 displays the shear stress distribution, while Table 4 lists recorded concrete shear stresses from FE simulations.

$$\tau_c = 0.17\sqrt{f'c} \quad \text{.... (1)}$$

Where τ_c is concrete shear stress.

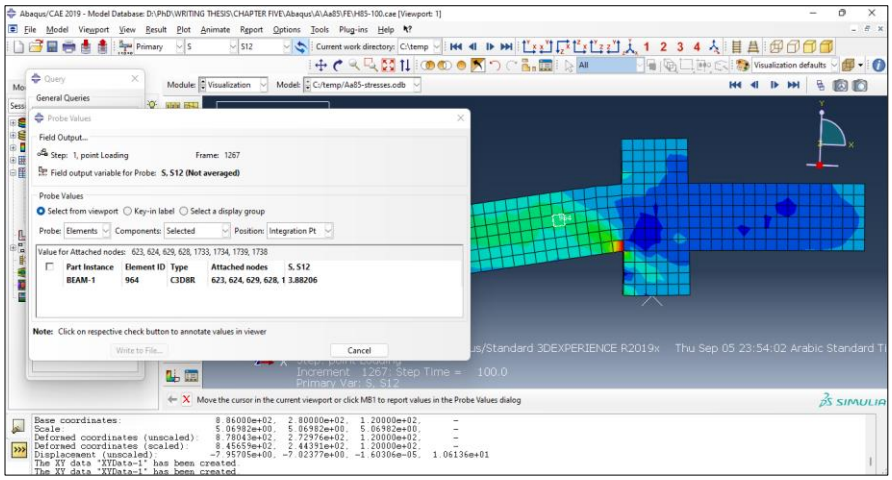

Figure 19. Values and distribution of shear stresses of Aa85 FE sample**.**

Table 4. Shear stresses of FE simulate sample.

Group	Sample	**Concrete Shear stresses** (MPa)	**ACI318-19* limit value (τ_c)**, (MPa)	**Shear strength of Concrete (V_c),** (kN)
A	Aa75	3.82	1.37	exhausted
	Aa85	3.8		exhausted
	Aa115	3.04		exhausted
B	Bs100	7.2		exhausted
	Bs150	5.45		exhausted
	Bs300	3.66		exhausted

*f'_c of all sample concrete is 65 MPa

Table 4 shows that the concrete's shear strength has been completely exhausted, resulting in V_c being zero.

12.2 Steel Shear Strength (Stirrups)

To analyze the role of stirrups in shear force resistance using S22 stresses in ABAQUS, focus on the stresses in the vertical stirrup legs. After running the simulation, extract the S11 stress values indicating normal stresses along the stirrup legs. Calculate the force for each leg by integrating these S11 stresses over the cross-sectional area. Sum the forces from all stirrups in the target area (plastic hinge region) to find the total shear force resisted and their contributions, as illustrated in Figure 20. Table 5 calculates the stirrups' contribution within each sample's target area.

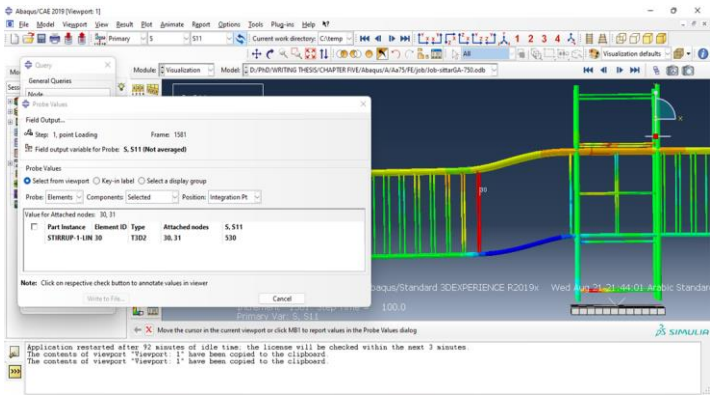

Figure 20. Evaluating shear stresses in stirrups**.**

Table 5. Stirrups' contribution and residual shear strength of steel

Group	Sample	*fvs* (Mpa)			*Avs* (mm2)	*Vsc** (kN)	*Vsn*** (kN)	*Vsr**** (kN)
		Stirrup-1	Stirrup-2	Stirrup-3				
	Aa75	530	0	0	56.52	29.96	29.96	0.00
A	Aa85	315			56.52	17.80	29.96	12.15
	Aa115	280	0	0	56.52	15.83	29.96	14.13
	Bs100	18	53	133	56.52	11.54	89.87	78.33
B	Bs150	83	109	0	56.52	10.80	59.91	49.12
	Bs300	176	0	0	56.52	9.95	29.96	20.01

*$V'sc=\sum fvsAvs$ (for all stirrups within the target area).
** *V'sn = d/s fsy * Avs (ACI318-19).*
*** *V'sr = V'sn -V'sc.*

Where:
f_{vs}: Stresses in the stirrups as recorded in the ABAQUS analysis.
A_{vs}: Cross-sectional area of the stirrup rebar (Two legs).
V_{sc}: Shear resistance contributed by the stirrups.
V_{sn}: Nominal shear resistance of the stirrups.
V_{sr}: Residual shear resistance of the stirrups.

As noted in Table 4, the shear resistance of the concrete has been completely used up. Consequently, the total shear capacity of the simulated specimens (V_{tr}) matches the residual capacity of the reinforcement (V_{sr}), as illustrated in the last column of Table 5.

13. Curvature Assessment

To evaluate the curvature of a steel-reinforced concrete (RC) beam, begin by measuring the horizontal displacements at the top and bottom surfaces at two cross-sections: the start and end of the target area (see Figure 21). Use Equation 2 below to calculate the rotation at each section [20].

$$\theta = \frac{u_{top} - u_{bottom}}{h} \quad \text{... (2)}$$

Where, u_{top} and u_{bottom} represent horizontal displacements, while h denotes the vertical distance (beam depth).

The curvature (φ) can be calculated from the change in rotation between the two sections and the distance separating them, as shown in the equation 3 below [21]:

$$\varphi = \frac{\theta_2 - \theta_1}{\Delta x} \quad \text{... (3)}$$

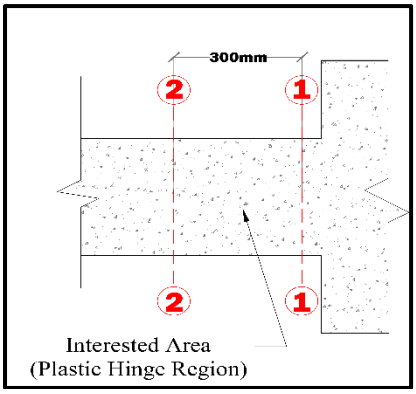

Figure 21. The two cross-sections positions.

Δx represents the horizontal distance between sections, while θ_1 and θ_2 denote the rotations at the start and end of the target area from the joint side, respectively. This method estimates beam curvature based on the rotations observed at two distinct sections [21].

Figures 22 to 23 show the curvature–moment relationship of all FE-simulating samples.

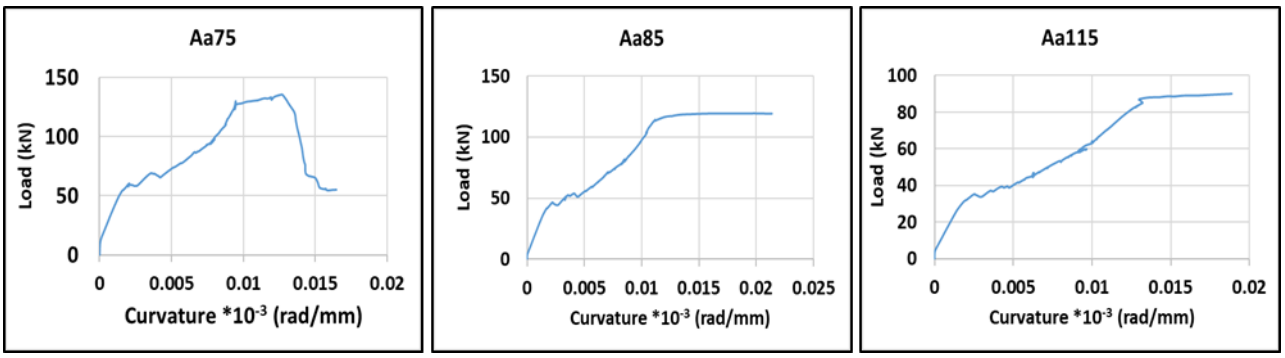

Figure 22. Moment-Curvature Relationship of group (A) samples.

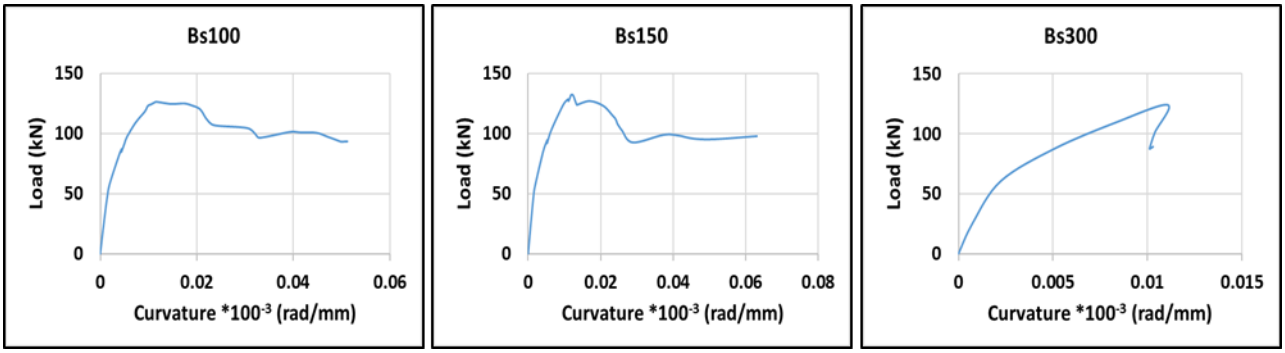

Figure 23. Moment-Curvature Relationship of group (B) samples.

14. Shear Capacity-Curvature Ductility Relationship

Curvature ductility is determined by correlating the beam's moment and curvature, which can be analyzed through the beam's cross-section while accounting for material nonlinearity and strain compatibility. The Curvature ductility index (μϕ) can be calculated as equation 4 and Figure 24 in chapter four.

$$\mu_\phi = \phi_u / \phi_y \quad \text{... (4)}$$

Where ϕ_y is the yield curvature and ϕ_u is the ultimate curvature.

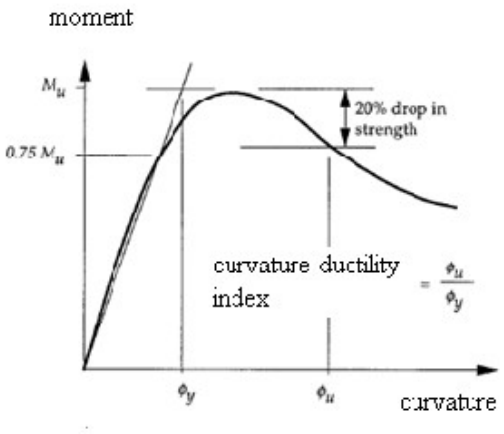

Figure 24. Determination of curvature ductility index [22].

The moment value at the yield point can be determined using two primary methods:

The Moment-Curvature Curve Method illustrates the relationship between moment and curvature in a structural member. The yield point indicates the transition from elastic to plastic behavior, marking the onset of plastic deformation and the moment of yielding [23].

The yield moment is generally estimated as 0.75 times the ultimate moment (Mu), a method widely endorsed by researchers [22]. This empirical approach offers a simplified estimate and is commonly used when detailed moment-curvature analysis is not available. The ultimate moment indicates the maximum moment a component can withstand before failure. Table 6 presents the curvature ductility index values for all beams tested using this method, as shown in Figures 22, 23, and 24.

Table 6. Curvature Ductility Index of all beams tested.

Group	Sample	ϕ_y *10^{-3} (rad/mm)	ϕ_u *10^{-3} (rad/mm)	μϕ
A	Aa75	0.0045	0.014	3.11111
	Aa85	0.0055	0.025	4.54545
	Aa115	0.0056	0.033	5.89286
B	Bs100	0.006	0.05	8.333
	Bs150	0.006	0.041	6.83333
	Bs300	0.004	0.0113	2.825

Table 7 and Figures 25 and 26 illustrate the shear capacity values and their relationship with the curvature ductility index for each group of FE-simulated samples.

Table 7. Shear Capacity and Curvature Index Values of FE-Samples**.**

Group	FE-Sample	Curvature Ductility	Shear Capacity (kN)
A	Aa75	3.11111	0
	Aa85	4.54545	12.15
	Aa115	5.89286	14.13
B	Bs100	8.334	78.33

	Bs150	6.83333	49.12
	Bs300	2.825	20.01

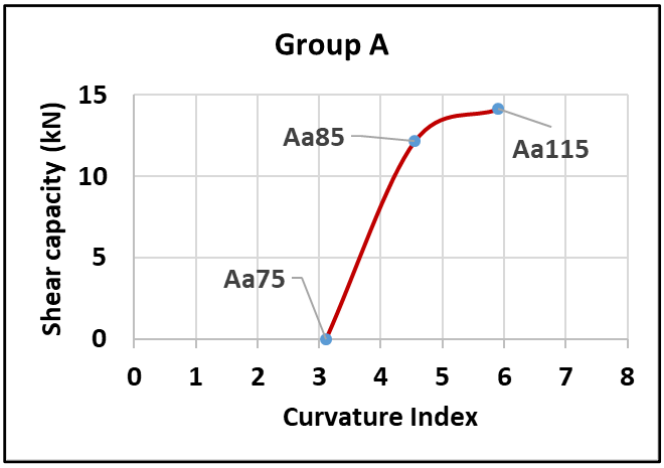

Figure 25. Shear Capacity – Curvature Ductility Relationships of FE-Samples of group A.

The investigation of group (A) revealed a direct relationship: as the shear span to effective depth ratio (a/d) increases, both the curvature ductility index and shear capacity rise. The relationship is characterized by two stages: a linear portion up to a specific value and a non-linear stage beyond that. This indicates that increased shear span enhances shear capacity only to a certain extent; beyond that point, additional increases have no effect on shear capacity.

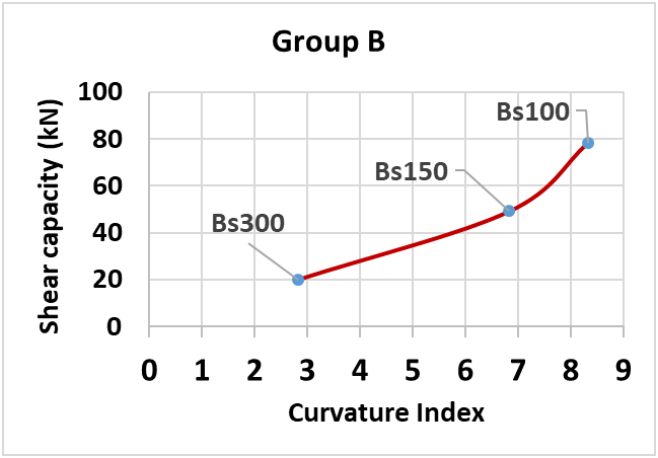

Figure 26. Shear Capacity – Curvature Ductility Relationships of FE-Samples of group B.

In Group B, the relationship is inverse and non-linear; as the spacing between stirrups increases, both the curvature ductility index and shear capacity of the samples decreases.

15. CONCLUSIONS

- A higher shear span to effective depth ratio (a/d) boosts a concrete beam's ductility and flexural deformability.
- Higher shear span-depth ratios (a/d) enhance flexural deformability, improving beam moment, deformability, and shear capacity pre-failure.
- Wider stirrup spacing may lower beams' curvature, shear capacity, and ductility, increasing failure risk.
- Diagonal shear stresses in the samples suggest potential concrete shear failure, mainly due to alignment with flexural cracks, accelerating their formation.
- Group (A) showed a direct relationship: as the shear span-to-depth ratio increases,

curvature ductility and shear capacity both increase.

- Group (A) has a relationship defined by two stages: a linear segment up to a certain value and a non-linear segment thereafter.
- For group B, the relationship is inverse and non-linear; as the spacing between stirrups increases, both the curvature ductility index and shear capacity of the samples decreases.
- Despite the designed failure modes being shear or bending, the samples exhibited a compound failure, suggesting that both types contributed to each other.

References

[1] Y.-F. Wu and B. Hu, "Shear strength components in reinforced concrete members," *Journal of Structural Engineering*, vol. 143, no. 9, p. 04017092, 2017.

[2] E. C. Bentz, F. J. Vecchio, and M. P. Collins, "Simplified modified compression field theory for calculating shear strength of reinforced concrete elements," *ACI Struct J*, vol. 103, no. 4, p. 614, 2006.

[3] A. Monserrat López, P. Miguel, J. Bonet Senach, and M. Prada, "Influence of the plastic hinge rotations on shear strength in continuous reinforced concrete beams with shear reinforcement," *Eng Struct*, vol. 207, p. 110242, Mar. 2020, doi: 10.1016/j.engstruct.2020.110242.

[4] A. L. L. Baker, *The Ultimate-load Theory Applied to the Design of Reinforced & Prestressed Concrete Frames*. in ("Concrete Series" Books on concrete and cement). Concrete Publications, 1956. [Online]. Available: https://books.google.iq/books?id=h4HTAAAAMAAJ

[5] H. A. Sawyer, "Design of Concrete Frames For Two Failure Stages," 1965. [Online]. Available: https://api.semanticscholar.org/CorpusID:114757218

[6] Corley W, "Rotational Capacity of Reinforced Concrete Beams," *Journal of the Structural Division*, vol. 92, no. 5, pp. 121–146, Oct. 1966, doi: 10.1061/JSDEAG.0001504.

[7] Mattock Alan, "Discussion of 'Rotational Capacity of Reinforced Concrete Beams,'" *Journal of the Structural Division*, vol. 93, no. 2, pp. 519–522, Apr. 1967, doi: 10.1061/JSDEAG.0001678.

[8] T. Paulay and M. J. N. Priestley, *Seismic design of reinforced concrete and masonry buildings*, vol. 768. Wiley New York, 1992.

[9] T. Panagiotakos and M. Fardis, "Deformation of Reinforced Concrete Members at Yielding and Ultimate," *ACI Struct J*, vol. 98, Mar. 2001.

[10] A. Mehta, R. Ravi, and S. Sivakamasundari, "Analytical Study of Plastic Hinge Formation in Beams Strengthened with CFRP Sheets," in *International Conference on Civil Engineering Innovative Development in Engineering Advances*, Springer, 2023, pp. 459–468.

[11] M. Srikanth, R. G., and S. Giri, "Moment curvature of reinforced concrete beams using various confinement models and experimental validation," *Asian J Civ Eng*, vol. 8, Jan. 2007.

[12] D. Dias-da-Costa, J. Valença, and R. Carmo, "Curvature Assessment of Reinforced Concrete Beams using Photogrammetric Techniques," *Mater Struct*, vol. 47, Jul. 2013, doi: 10.1617/s11527-013-0148-8.

[13] H. T. Jaber, K. F. Sarsam, and B. R. Muhammad, "Numerical study on the shear strength of reinforced concrete beams using ABAQUS," in *AIP Conference Proceedings*, AIP Publishing, 2023.

[14] H. H. Hussein, K. K. Walsh, S. M. Sargand, and E. P. Steinberg, "Interfacial properties of ultrahigh-performance concrete and high-strength concrete bridge connections," *Journal of Materials in Civil Engineering*, vol. 28, no. 5, p. 04015208, 2016.

[15] A. H. Mohammed, Q. A. Hasan, and K. F. Sarsam, "The influence of RPC thickness on hybrid beams under torsion," in *IOP Conference Series: Materials Science and Engineering*, IOP Publishing, 2020, p. 012027.

[16] L. Chen and B. A. Graybeal, "Modeling structural performance of ultrahigh performance concrete I-girders," *Journal of Bridge Engineering*, vol. 17, no. 5, pp. 754–764, 2012.

[17] T. Wang and T. T. C. Hsu, "Nonlinear finite element analysis of concrete structures using new constitutive models," *Comput Struct*, vol. 79, no. 32, pp. 2781–2791, 2001.

[18] P. Kmiecik and M. Kamiński, "Modelling of reinforced concrete structures and composite structures with concrete strength degradation taken into consideration," *Archives of civil and mechanical engineering*, vol. 11, no. 3, pp. 623–636, 2011.

[19] U. Florida, "Von Mises Yield Criterion for Steel Rebar Failure Prediction," 2024. [Online]. Available: https://mae.ufl.edu/nkim/eas4200c/VonMisesCriterion.pdf

[20] J. G. MacGregor, J. K. Wight, S. Teng, and P. Irawan, *Reinforced concrete: Mechanics and design*, vol. 3. Prentice Hall Upper Saddle River, NJ, 1997.

[21] W. A. Aules, F. Rad, P. Dusicka, T. Schumacher, and H. Zareh, "Behavior of Non-Ductile Slender Reinforced Concrete Columns Retrofit by CFRP under Cyclic Loading," 2019.

[22] M. T. Desai Pallavi and A. Rajan Professor, "'SEISMIC PERFORMANCE OF SOFT STOREY COMPOSITE COLUMN,'" *Int J Sci Eng Res*, vol. 4, no. 1, 2013, [Online]. Available: http://www.ijser.org

[23] B. Haytham and K. Amar, "Curvature Ductility of High Strength Concrete Beams," 2017.